Engineering Geology 309 (2022) 106828

Contents lists available at ScienceDirect

Engineering Geology

journal homepage: www.elsevier.com/locate/enggeo

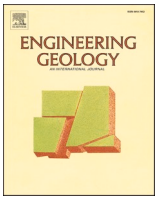

Estimating rockfall and block volume scenarios based on a straightforward rockfall frequency model

Christine Moos [a,*], Zeno Bontognali [b], Luuk Dorren [a], Michel Jaboyedoff [c], Didier Hantz [d]

[a] Bern University of Applied Sciences – HAFL, Zollikofen, Switzerland
[b] Egli Engineering AG, Bern/St. Gallen, Switzerland
[c] Risk Group, University of Lausanne, Lausanne, Switzerland
[d] Univ. Grenoble Alpes, Univ. Savoie Mont Blanc, CNRS, IRD, Univ. Gustave Eiffel, ISTerre, 38000 Grenoble, France

ARTICLE INFO

Keywords:
Rockfall
Rockfall frequency
Power law
Block size distribution
Risk assessment

ABSTRACT

Rockfall causes a large number of accidents and fatalities in steep environments. A realistic quantification of rockfall risk is thus crucial for an effective prevention of damages and loss of lives. The estimation of rockfall and block volumes for different return periods thereby remains a major challenge. In this paper, we present a straightforward rockfall frequency model (RFM: Rockfall Frequency Model) and its application at 8 different sites at 7 locations in the Swiss Alps. The RFM assumes that the magnitude-frequency relationships of rockfall events and blocks follow a power law. The parameters of this distribution are estimated based on a simple classification of rock structures and on field inventories. Beside the block volume frequency, which is very sensitive to the consideration of large rockfall events, the frequency of rockfalls with at least one block with a minimum volume, is determined. The block size distributions measured in this study were well captured by power laws. The rockfall and block volumes calculated with the RFM were generally slightly higher than the scenarios of the official hazard assessments. The uncertainty analysis, however, revealed a high variability of the release scenarios with respect to the parameters of the RFM, increasing with the return period. Both, the rockfall volumes and the block volumes, are particularly sensitive to the estimated exponent of the power law distribution of the rockfall events. Nevertheless, the proposed RFM provides an objective and transparent approach to derive magnitude-frequency relationships of rockfall events and individual blocks even if historical inventories are missing or insufficient and is thus a promising alternative to merely expert-based approaches.

1. Introduction

Rockfall is a frequent natural hazard in steep, mountainous environments endangering settlements and infrastructure (Guzzetti, 2000; Loew et al., 2021). Its occurrence is affected by many uncertainties and thus hardly predictable. For this reason, together with the generally high impact intensities, rockfall causes high costs compared to other landslide types (Arnold and Dorren, 2015; Ferrari et al., 2016). A realistic quantification of rockfall risk is crucial for an effective and efficient prevention of economic damages and loss of lives. Although rockfall trajectory models allow for an increasingly precise calculation of rockfall runout zones and the kinetic energies of blocks (Agliardi and Crosta, 2003; Bourrier et al., 2009; Dorren et al., 2006; Christen et al., 2012), the estimation of realistic block and event volumes as well as their release frequencies remain a major challenge. They are often based on one or several scenarios which represent estimates of different event magnitudes (release volumes) and return periods, based on geological surveys of the rock cliff and (scarce) inventory data. In the past, a few analyses of rockfall frequencies based on long-term historical inventories have been published (e.g., Hungr et al., 1999; Dussauge-Peisser et al., 2002; Eckert et al., 2020; Melzner et al., 2020). De Biagi et al. (2017) combined the analysis of available historical data with a survey of detached blocks in a probabilistic method to determine the rockfall magnitude-frequency relationship. The problem with inventory data is that i) observation periods are often short and thus the statistical representativeness is questionable (Hantz et al., 2020) and that ii) they are usually registered at the element at risk and often only in case of damages and, thus, rather represent the occurrence frequency at the element at risk than the release frequency. However, release frequencies are required to realistically quantify the rockfall risk for a specific

* Corresponding author.
E-mail address: christine.moos@bfh.ch (C. Moos).

https://doi.org/10.1016/j.enggeo.2022.106828
Received 1 March 2022; Received in revised form 6 July 2022; Accepted 10 August 2022
Available online 16 August 2022
0013-7952/© 2022 The Author(s). Published by Elsevier B.V. This is an open access article under the CC BY license (http://creativecommons.org/licenses/by/4.0/).

source: https://doi.org/10.24451/arbor.18112 | downloaded: 21.12.2022

element at risk and for a variation of propagation settings (e.g., with or without protection measures) (Lari et al., 2014; Moos et al., 2018). Other approaches are based on the analysis of remotely sensed data (e.g., Guerin et al., 2014; van Veen et al., 2018; Umili et al., 2020) or dendrogeomorphological analyses (Mainieri et al., 2019; Stoffel et al., 2005). Farvacque et al. (2021) proposed a method to estimate rockfall release frequency combining field-based data from rockfall protection barriers and tree-ring records of past rockfall activity with process-based modeling approaches. They found a good agreement between release frequencies determined from tree-ring analyses and obtained from rock deposits in the protection barriers. However, the mentioned approaches are often very cost- and time-intensive and/or rely on a large amount of (often unavailable) data and are, thus, not applicable in current practice. Engineering consultancies in charge of hazard assessments are generally limited in time and resources and thus rely on straightforward approaches and methods to determine rockfall release frequencies. These, however, often sacrifice in accuracy and objectivity.

Based on the analysis of the rockfall frequency and magnitude in a range of rock cliffs, Hantz et al. (2020) and Loew et al. (2021) proposed a power law based model for the determination of rockfall magnitude-frequency relationships aiming at a more objective approach for practitioners. It assumes that both, the releasing masses of rockfall events as well as the individual blocks of a rockfall event resulting from first fracturing follow a power law distribution. The parameters of these distributions are determined using a simple classification of rock structure in combination with field measurements of blocks. In this study, we applied and tested the proposed rockfall frequency model (RFM) at 8 different sites at 7 locations in the Swiss Alps. The calculated frequencies of rockfall events and the derived block volumes were compared to release scenarios of official hazard assessments. Additionally, the sensitivity and uncertainty of the derived rockfall scenarios regarding the parameters of the RFM were assessed.

2. Rockfall frequency model

The frequency of the detachment of rockfall events (hereafter called "release frequency") is subject to a wide range of uncertainties and can hardly be predicted in a deterministic way. Thus, statistical models are often used to approximate the onset frequency of a rockfall event of a given size. Power law distributions have been proven to fit well the magnitude-frequency relationship of the released rockfall events and the released blocks, respectively (Hungr et al., 1999; Dussauge-Peisser et al., 2002). The spatio-temporal release frequency of rockfall events (introduced by Hantz et al., 2003a) can be expressed as:

$$F_{st}(V) = A_{st} V^{-B} \tag{1}$$

$F_{st}(V)$ is the number of rockfall events releasing per year and hectare. A_{st} represents the activity of the rock cliff and corresponds to the frequency of rockfall events with a volume > 1 m^3 per hectare of the rock cliff. B characterizes the volume distribution and depends on the geological structure. It mainly varies between 0.4 and 0.8 (Brunetti et al., 2009). Eq. 1 applies up to a maximum possible rockfall volume, which depends on the size and the geological structure of the rock cliff.

By multiplying F_{st} with the surface S of the rock cliff, we get the temporal frequency of the considered cliff $F_t(V)$:

$$F_t(V) = \mathrm{S} \times A_{st} V^{-B} \tag{2}$$

The volume of a rockfall can be determined by comparing the pre-failure and post-failure surfaces in the cliff or by estimating the volume of the deposit of an event. A rockfall event is defined as the detachment of a rock volume between two different points in time. Van Veen et al. (2017) and Williams et al. (2019) pointed out that neighboring events occurring within a single monitoring interval are often recorded as one. Thus, the volumes of the rockfalls occurred in a cliff and their distribution depend on the monitoring interval, which must be considered by the users of a rockfall volume-frequency relation.

A rockfall event is generally composed of fragments. The volume distribution of these single blocks can also be approximated with a power law distribution (e.g., Hantz et al., 2016; Ruiz-Carulla et al., 2017; Moos et al., 2018):

$$f_{st}(v) = a_{st} v^{-b} \tag{3}$$

where f_{st} is the release frequency of blocks per year and hectare. The parameter a corresponds to the number of blocks larger than 1 m^3 per year and hectare. The uniformity parameter b is generally larger than the parameter B of the event distribution (between 0.5 and 1.5; Mavrouli et al., 2015).

2.1. Frequency distribution of blocks

By integrating the volume-frequency relationship of the rockfall events over the frequency with consideration of a maximum possible rockfall volume, the retreat rate R of the cliff can be calculated (Eq. 4; Hantz et al., 2003b, 2020). The latter describes the total eroded volume of a cliff per time and surface of the cliff (in mmyr^{-1}). It is usually assessed based on inventory data (e.g., Allen et al., 2011), comparisons of historical and recent photographs (e.g., Ravanel and Deline, 2010) or laser scanning (e.g., Mohadjer et al., 2020).

$$R = \frac{A_{st}}{(1-B)} V_{MAX}^{(1-B)} - \frac{A_{st} B}{(1-B)} V_{MIN}^{(1-B)} \tag{4}$$

V_{MIN} is the minimum considered volume and V_{MAX} the maximum possible volume. By considering a maximum possible rockfall volume, rare events are taken into account (assuming the power law is valid up to this volume). Analogously, the retreat rate can be calculated from the volume-frequency relationship of the block volumes:

$$R' = \frac{a_{st}}{(1-b)} v_{MAX}^{(1-b)} - \frac{a_{st} b}{(1-b)} v_{MIN}^{(1-b)} \tag{5}$$

With v_{MAX} being the maximum possible block volume and v_{MIN} the minimum considered block volume. The integration of the block volumes is not always convergent for a volume of 0 m^3 (because b can be bigger than 1) and, thus, minimum block and event volumes have to be determined. In case the parameters A_{st}, B, V_{MAX} and b are known, the parameter a_{st} can be calculated by equating the two retreat rates:

$$\mathrm{ast} = \frac{R(1-b)}{v_{MAX}^{(1-b)} - b v_{MIN}^{(1-b)}} \tag{6}$$

The above explained model allows for characterizing the frequency distribution of block volumes. It is an "overall frequency" including the blocks theoretically falling during all potential rockfall events. It is obvious that the large number of blocks in the very big and rare events strongly influence the block volume frequency. This exemplifies that block releases are not independent events, and their onset probability cannot be modelled using a Poisson or binomial distribution (Hantz et al., 2021).

2.2. Frequency of rockfall events and maximum block volumes

Besides the overall release frequency of blocks, the frequency of rockfall events including at least one block of a given minimum volume or, inversely, the maximum block volume for a given rockfall frequency are of particular interest in hazard management. For this, it is necessary to determine the maximum probable block volume (and the number of blocks of this volume) as a function of the rockfall event volume.

The volume V of a rockfall event can be obtained by integrating the volumes of the individual blocks between a minimum volume v_{MIN} and the maximum possible volume v_{MAX} (regardless of V; Eq. 7). The minimum block volume must be strictly positive since the integral would not converge for $b > 1$ if $v_{MIN} = 0$. Thus, we assume that the rockfall volumes

are estimated by counting only the blocks with volumes bigger than v_{MIN}.

$$V = \frac{a}{(1-b)} v_{MAX}^{(1-b)} - \frac{ab}{(1-b)} v_{MIN}^{(1-b)} \quad (7)$$

For a given rockfall volume V and a known b value, the parameter a is:

$$a = \frac{V(1-b)}{v_{MAX}^{1-b} - b v_{MIN}^{1-b}} \quad (8)$$

By calculating the parameter a for a given rockfall volume V and b value, the block volume distribution can be known. If $n(v_{MAX}) > 1$, the number of blocks with volume v_{MAX} in the rockfall event is the integer part of $a^* v_{MAX}^{-b}$. If $n(v_{MAX}) < 1$, the biggest occurring block has a volume $v_{max}(V) = a^{1/b}$, which is lower than v_{MAX} (Fig. 1).

In hazard and risk analysis, rockfall and block volumes are usually required for a set of scenarios of different return periods (or frequencies). The rockfall volume of a given frequency F_t can be calculated based on the rockfall frequency distribution (Eq. 2):

$$V(F_t) = \left(\frac{Ast^*S}{F_t}\right)^{1/B} \quad (9)$$

Note that $V(F_t)$ is a function of B that is decreasing if $(A_{st}{}^*S/F_t) > 1$ or increasing if $(A_{st}{}^*S/F_t) < 1$. It must be checked that $V(F_t)$ is smaller than the maximum possible rockfall volume (V_{MAX}).

For the rockfall volume of frequency F_t, the number of blocks of v_{MAX} (in case $n(v_{MAX}) > 1$) or the volume of the largest occurring block v_{max} (in case $n(v_{MAX}) < 1$) can then be calculated. In this study, we calculated event and block volumes for four return periods of 10 yrs. ($F_t = 1/10$), 30 yrs. ($F_t = 1/30$), 100 yrs. ($F_t = 1/100$) and 300 yrs. ($F_t = 1/300$).

3. Methods

3.1. Parameter estimation

3.1.1. Maximum possible rockfall volume and maximum block volume

The maximum possible volume of a rockfall V_{max} has to be considered if the rockfall volume-frequency relationship is extrapolated to rare events. It depends on the size of the rock wall (height, width), its morphology (slope angle and aspect) and on the structure of the rock mass (dips, dip direction, size and spacing of the discontinuities). Corominas et al. (2018) presented two standard approaches to assess the maximum possible (or credible) rockfall event, which can be bigger than the largest event of a potentially available historical inventory. The first one (inductive) consists in searching morphological evidence of passed rockfall events (deposits and scars left at the source). It allows for considering a period that is longer than the one covered by the historical inventory, but which is nevertheless limited. The second approach (deductive) consists in defining the maximum rockfall volume from the available data on the topography and internal structure of the rock cliff. The structure can be considered either statistically (identification of discontinuity sets) or deterministically (identification of individual potential sliding planes). Examples are given in Jaboyedoff et al. (2009), Mavrouli et al. (2015), Corominas et al. (2018) and Jaboyedoff et al. (2020).

Here we propose a simple method based on Hoek and Bray (1981) to be used when the geological structure is barely known. The model assumes a critical plane (or wedge) that outcrops at the base of the slope and a simplified geometry of the slope to determine the maximum possible volume of a slide. The critical sliding surface can be determined from a structural analysis of the rock mass (Fig. 2a). When there is no structural analysis, we assume that sliding may occur on a plane having the minimum dip (to maximize the sliding volume), but which is sufficient for sliding to occur (Fig. 2b). We propose values of this "minimum slide dip" based on the surface condition of the potential sliding plane (or wedge) as defined by Hoek and Marinos (2000), Marinos and Hoek (2001) and Hoek et al. (2005) (Table 1). It can be adjusted based on expert judgment. It is important to note that for sliding planes with low dips (10°- 20°), the hypothesis of an infinite extension is too conservative because a tension crack usually bounds the sliding mass. The width of the biggest possible slide is assumed to equal the rock wall height, since a plane slide is rarely much wider than height (Frayssines and Hantz, 2006). Rockfall may also result from a topple. However, it can be assumed that the maximum rockfall volume resulting from a topple is smaller than the maximum rockfall volume resulting from a slide. It has to be noted that the simple method proposed here is conservative and may also include rockslides in the scenarios. The latter typically show another behavior compared to rockfall and, thus, should be treated separately in risk assessments. However, the maximum event volume predominantly influences the overall block frequency in the proposed model (Eq. 4–6), but it does not influence the calculation of the rockfall event volumes of a given return period and the associated number of blocks (Eq. 8–9) as it was applied in this study.

The maximum block volume was estimated by expert judgment based on the block volume samples measured in the field and inventory data of past rockfall events. It could also be estimated based on the structure of the rock mass (Mavrouli et al., 2015).

3.1.2. Parameters A_{st} and B

The parameter A_{st} shows the activity of the cliff and B determines the uniformity of the rockfall volume distribution and depends on the rock wall structure. It was determined following the classification proposed by Hantz et al. (2020), who analyzed the rockfall frequency in anaclinal limestone cliffs and a gneissic cliff in non-permafrost areas of the Alps. The rockfall frequencies in these cliffs were at such a low level that very

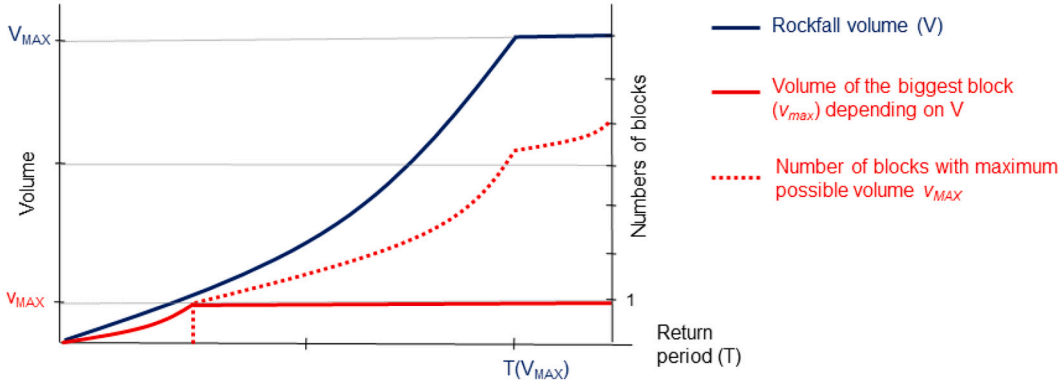

Fig. 1. Schematic characterization of the rockfall volume (V), the volume of the biggest block (v_{max}) and the number of blocks with the maximum possible volume (v_{MAX}) in a rockfall as a function of the return period T. Note: These do not depend on V_{MAX} when $T < T(V_{MAX})$.

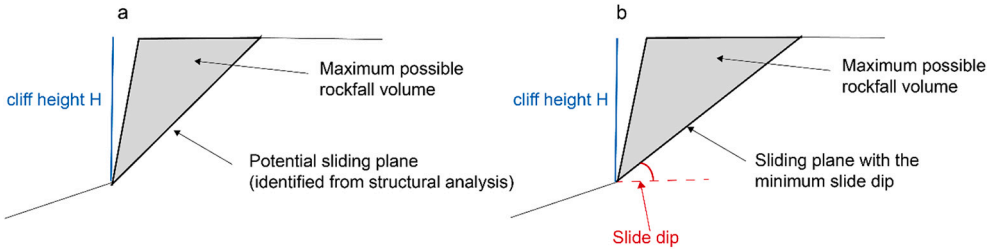

Fig. 2. The potential sliding plane is determined from a structural analysis if available (a). In this study, the sliding plane with the minimum slide dip was considered since no structural analysis was available. The minimum slide dip was determined according to the surface conditions (Table 1).

Table 1
Determination of the minimum slide dip according to a categorization of the surface conditions (based on Hoek and Marinos (2000), Marinos and Hoek (2001), Hoek et al. (2005)).

Surface conditions	Minimum slide dip
Very good (very rough, fresh and unweathered surfaces)	40°
Good (rough, slightly weathered, iron stained surfaces)	35°
Fair (smooth, moderately weathered and altered surfaces)	30°
Poor (slickensided, highly weathered surfaces with compact coatings or fillings or angular fragments)	20°
Very poor (slickensided, highly weathered surfaces with soft clay coatings or fillings)	10°

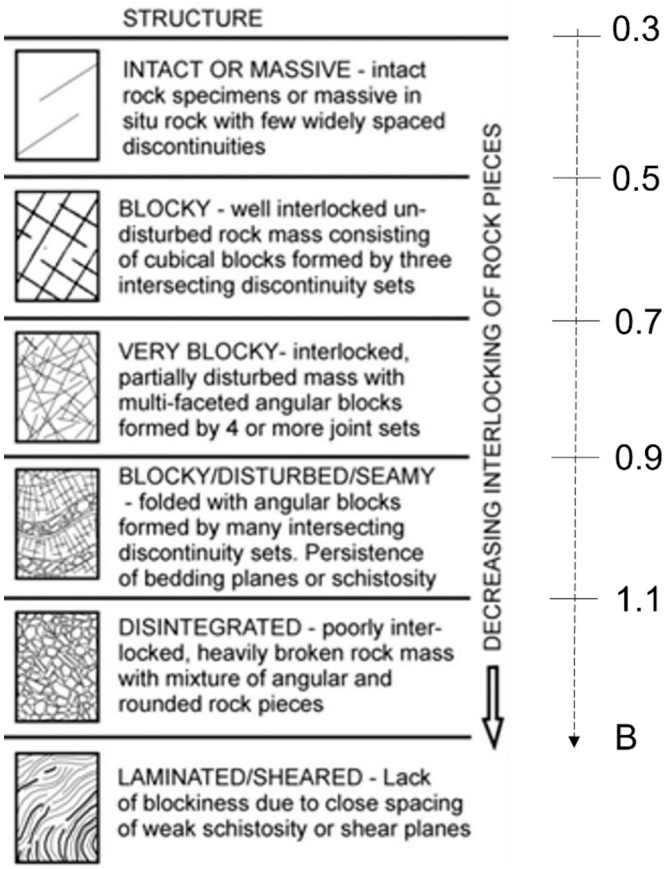

Fig. 3. Estimation of parameter B based on a classification of the rock structure. The associated uncertainty is estimated to one class width (+/− 0.2) based on Hantz et al. (2020). The structure types are derived from Hoek (2007). Figure adapted based on Hoek (2007) and Hantz et al. (2020).

few neighboring events were recorded as one with a monitoring interval of one year. In the classification, six main structure types are distinguished (Fig. 3). The parameter A_{st} depends on the spacing of the main joint set of the rock wall (Hantz et al., 2020). The analyses of inventory data imply that a metric distance of the spacing corresponds to a A_{st} value between 0.01 and 0.1 and a decimetric distance to a A_{st} value between 0.1 and 1. A_{st} can be estimated using the following equation (Hantz et al., 2020):

$$A_{st} = 10^{-log(10*s)} \quad (10)$$

whereas s is the average spacing of the main joint set in the rock wall.

3.1.3. Parameter b

The uniformity parameter b of the block volume distribution was determined based on block volume samples collected in the field. For each case study site, we sampled blocks along transects in the deposition area. Depending on the size of the deposition area, one or several downslope transects following the mean trend of trajectories with a length of 20 m were determined, aiming at a realistic representation of the block size distribution including areas with smaller and larger blocks (following Ruiz-Carulla et al., 2015; Fig. 4). Along this transect, all blocks with a volume ≥ 0.05 m^3 were measured for a transect width of 2 m. To calculate the volume of a block, we measured three edges of the block and determined a correction factor (f) for the block volume compared to a perfect cube. For Orvin and Täsch, we used already available block samples from a recent study (Moos et al., 2018). We then fitted a power law distribution to the measured volumes based on least squares to derive parameter b. The degree of precision of the estimates of the parameter b was determined through a bootstrap analysis (Bengoubou-Valérius and Gibert, 2013; De Biagi et al., 2017). We fitted the parameter b for 10′000 bootstrap samples of the block volumes and determined the 95%-confidence intervals of the estimates.

3.2. Test sites

The RFM was elaborated and tested for eight rock cliffs at seven locations in Switzerland (Fig. 5). The sites were selected based on the following criteria:

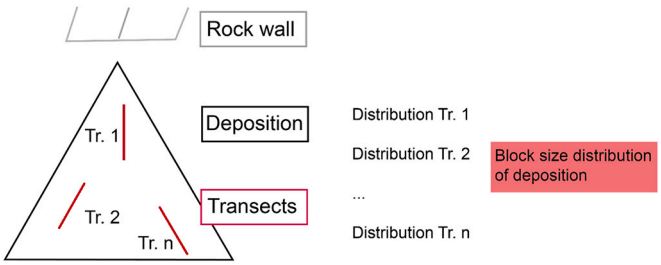

Fig. 4. Block size distributions were determined based on block samples along transects in the deposition area. Blocks with a volume ≥ 0.05 m^3 were measured.

Fig. 5. Overview of the test sites. In Fläsch, two different rock cliffs were analyzed.

i) The rock cliffs have different lithologies;
ii) There are block deposits on the slope;
iii) There are existing official hazard assessments available and if possible, inventory data on past events.

Three of the sites are in the canton of Valais (Swiss Western Alps), one in the canton of Bern (Jura), one in the canton of Grisons (Swiss Eastern Alps) and two in the canton of Ticino (Swiss Southern Alps). The main characteristics and available data are summarized in Table 2. The scenarios of the official hazard assessment are mainly expert based with large differences in the underlying data basis. Images of the release areas can be found in Appendix A.

3.3. Sensitivity and uncertainty analysis

We quantified the uncertainty and sensitivity regarding the parameters A_{st}, B, b, V_{MAX} and v_{MAX} and the surface of the cliff S for the calculated release scenarios based on a Monte Carlo approach. We determined the following "error margins" for the parameters based on expert judgment:

A_{st}: variation by a factor 2 ($1/2*A_{st}$ - $2*A_{st}$).

B: variation by +/− 0.2 (one class width; Fig. 3).

S: Variation by +/− 20%.

b: variation between lower and upper bound of the bootstrap confidence intervals (see section 2.3.3).

v_{MAX}: variation by +/− 30%.

V_{MAX}: variation by – 50% (calculated V_{max} is regarded as the upper possible limit).

At each iteration of the Monte Carlo analysis, parameter values were randomly sampled from these ranges following a uniform distribution and the rockfall volume ($V(F_t)$) and the maximum block volume v_{max} (F_t) were calculated. This was repeated 10,000 times. Finally, we calculated the mean, median and standard deviation of the derived rockfall event and block volumes.

Table 2
Description of the test sites used in this study with the estimated spacing of the main joint set (s) and the block/event scenarios of the official hazard assessments.

Site	Main lithology	Cliff surface S [ha] and average cliff height [m]	estimated spacing of the main joint *s* [m]	Block/event scenarios of the official hazard assessments with return period (1 = 10 yrs.; 2 = 30 yrs.; 3 = 100 yrs., 4 = 300 yrs)	Other sources than official hazard analyses
Bodio	Ortho gneiss	9.4/80	0.3–0.4	0.4 m^3 (1); 3.0 m^3 (2); 20 m^3 (3); 270 m^3 (4)	–
Fläsch 1	Siliceous limestone	21.9/50	0.1–0.2	10.3 m^3 (1); 15 m^3 (2); 21 m^3 (3); 256 m^3 (4)	–
Fläsch 2	Limestone breccia	3.7/50	0.1–0.2	1.125 m^3 (1); 2.25 m^3 (2); 5 m^3 (3); 256 m^3 (4)	–
Morcote	Ortho gneiss	0.3/20	0.2–0.3	Hazard assessment without release scenarios	–
Nax	Dolomite	3.7/100	0.1–0.2	0.3 m^3 (1); 0.3 m^3 (2); 2–4 m^3 (3); 2–4 m^3 (4)	–
Orvin	Bioclastic limestone	1.7/100	0.3–0.4	0.5 m^3 (1); 1.2 m^3 (2); 4 m^3 (3); 9 m^3 (4)	Release frequencies derived from dendrogeomorphological analyses (Moos et al., 2018)
Simplon	Ortho gneiss	8.3/100	0.3–0.4	0.1 m^3 (1); 0.5 m^3 (2); 150 m^3 (3); 150 m^3 (4)	–
Täsch	Amphibolite/ gneiss	17 /100	0.2–0.3	5–10 m^3 (1); 5–10 m^3 (2); 10–20 m^3 (3)	Release frequencies derived from dendrogeomorphological analyses and deposits in rockfall barriers (Moos et al., 2018)

To determine the contribution of each parameter to the overall output uncertainty, we used the least square linearization (LSL; Lei and Schilling (1996)). LSL splits output uncertainty into its sources based on a multiple regression between the parameter deviation from the mean and the output (Verbeeck et al., 2006). It enables calculating uncertainty coefficients of all parameters, based on which they can be ranked regarding their influence on the overall output uncertainty.

3.4. Comparison to hazard scenarios

A major challenge of implementing the RFM is its validation since data on past events is generally missing or of insufficient quantity or quality. The rockfall release scenarios determined in this study were compared to i) release scenarios of official hazard analyses determined by engineering consultancies; ii) release frequencies determined based on a combination of dendrogeomorphological analyses and rockfall deposits published in a recent study for the sites Orvin and Täsch (Moos et al., 2018). The available data and applicable validation approaches per site are summarized in Table 2.

4. Results

4.1. Parameter estimations

The parameter A_{st} was estimated between 0.05 yr^{-1} ha^{-1} (Bodio; Table 3) and 0.3 yr^{-1} ha^{-1} (Fläsch 1 & 2; Nax). The parameter B ranged between 0.5 (Bodio) and 0.9 (Nax). The maximum possible volumes were estimated between 8000 m^3 (Morcote) and 680′000 m^3 (Nax; Table 3).

The block size distributions of all sites were well captured by the power law distributions (R^2 between 0.82 and 0.98). The fitted b values vary between 0.69 (Bodio; Table 3 and Fig. 6) and 1.69 (Nax). The uncertainty associated with the b estimates, as represented by the bootstrap confidence intervals in Table 3, substantially increases with decreasing block sample size (e.g., Morcote and Nax). There seems to be a tendency that b values are higher for limestone and dolomite compared to gneiss. Furthermore, b tends to increase with increasing B (Fig. 7).

4.2. Release scenarios

The calculated block and event scenarios are reported in Table 4 and Fig. 8-10 for the different return periods. For the small return periods, the block sizes are usually in a comparable range with the scenarios of the official hazard assessment, but generally slightly larger. The difference increases with the return period (Fig. 8). For all sites, the standard deviations calculated by means of the Monte Carlo simulations are relatively high, indicating a large parameter sensitivity (Table 4). The variability of the event and block volumes also substantially increases with the return period (Figs. 9 & 10). For certain sites, the maximum possible block volume is already reached for return periods of 30–100 years, leading to an "asymptotic" trend in Fig. 10 (e.g., Fläsch 1 or Bodio). Tthe highest sensitivity of the block volumes was found to parameter B and partially the parameter A_{st} as well as the cliff size for return periods of 100 and 300 years. The event volumes are also most sensitive to parameter B except for the sites of Morcote and Orvin (Fig. 11).

Table 3
Estimated values per site for the parameters A_{st}, B, b, v_{MAX} and V_{MAX} of the RFM. for parameter b The 95% bootstrap confidence interval (conf.b) and the block sample size (n) is given in brackets.

Site	A_{st} [yr^{-1} ha^{-1}]	B	V_{MAX} [m^3]	b (conf.b) (n)	v_{MAX} [m^3]
Bodio	0.05	0.5	290′000	0.69 (0.63, 0.79) (70)	300
Fläsch 1	0.3	0.8	70′000	0.77 (0.71, 0.84) (50)	50
Fläsch 2	0.3	0.8	70′000	1.45 (1.40, 1.50) (118)	20
Morcote	0.2	0.8	8′000	0.93 (0.73, 1.07) (5)	20
Nax	0.3	0.9	680′000	1.69 (1.59, 1.92) (21)	20
Orvin	0.1	0.8	570′000	1.05 (0.99, 1.10) (209)	20
Simplon	0.1	0.7	570′000	0.93 (0.89, 0.98) (82)	50
Täsch	0.15	0.8	570′000	1.04 (1.01, 1.07) (1313)	50

5. Discussion and conclusion

Determining realistic rockfall release frequencies is crucial for an adequate assessment of rockfall risk. Practitioners derive rockfall release scenarios often rather subjectively and uniform approaches and concepts are generally missing. The rockfall frequency model (RFM) applied in this study provides an objective and transparent approach to derive magnitude-frequency relationships of rockfall events and individual blocks even if historical inventories are missing or insufficient. It also allows for the determination of the frequency of rockfalls with at least one block with a minimum volume. It is a promising alternative to merely expert-based approaches for the following reasons: i) It requires only few parameters that are estimated based on simple schemes. This is a perfect precondition for its practical implementation; ii) the RFM assumes that the magnitude-frequency relationships for rockfall events and the individual blocks of an event can be characterized by a power law distribution. A wide range of studies evidence that this assumption is rather realistic (e.g., Hungr et al., 1999; Dussauge-Peisser et al., 2002; Ruiz-Carulla et al., 2015; Hantz et al., 2016), implying that the resulting frequencies are reliable. The comparison to the official hazard assessments in this study showed that this is not necessarily the case for the expert-based rockfall scenarios, where volume distributions were partially rather arbitrary; iii) the RFM provides an explicit quantification of the release frequency, whereas approaches based on inventories at the element at risk (e.g., De Biagi et al., 2017) only allow for the determination of the occurrence frequency at the elements at risk. Knowing the release frequency enables evaluating rockfall risk for different propagation scenarios, which is particularly relevant for hazard and risk assessments evaluating protection measures.

The block volume distributions of all study sites were well represented by power law distributions, indicating the scale invariant character of rock fragmentation (Turcotte, 1986). The fitted b values lay in a range that is similar to the range reported by Hantz et al. (2020) (0.47, 1.37), except the b value for Nax that is significantly higher (1.69). This suggests that dolomite gives a more uniform block volume distribution than the other rocks reported by Hantz et al. (2020). Two sites (Nax, Fläsch 1) have higher b values compared to the range (0.63–1.29) obtained by Lanfranconi et al. (2020), who also found a different trend in the lithology dependence. The value of the parameter b depends mainly on the geology of the cliff, and fragmentation is often caused by fracturing along pre-existing weak joint planes (e.g., Lin et al., 2022). Additionally, the fall height of the blocks plays a role (De Blasio and Crosta, 2015; Ruiz Carulla et al., 2016). Surprising is the large difference of the b values of the two neighboring sites Fläsch 1 ($b = 0.77$) and 2 ($b = 1.45$). They, however, differ in their lithology, which could explain the differing fragmentation behavior. While Fläsch 1 is composed of siliceous limestone (with partly marly rocks), Fläsch 2 is composed of limestone breccia and marly rocks. Furthermore, the block sample size of Fläsch 1 is distinctly smaller than for Fläsch 2, which could have led to a bias in the estimation.

The method used in this study for taking block samples in the field is a simplification of the approach proposed by Ruiz-Carulla et al. (2015). It is little time-consuming, easy to implement and requires only a couple of hours per site, depending on the site characteristics and accessibility

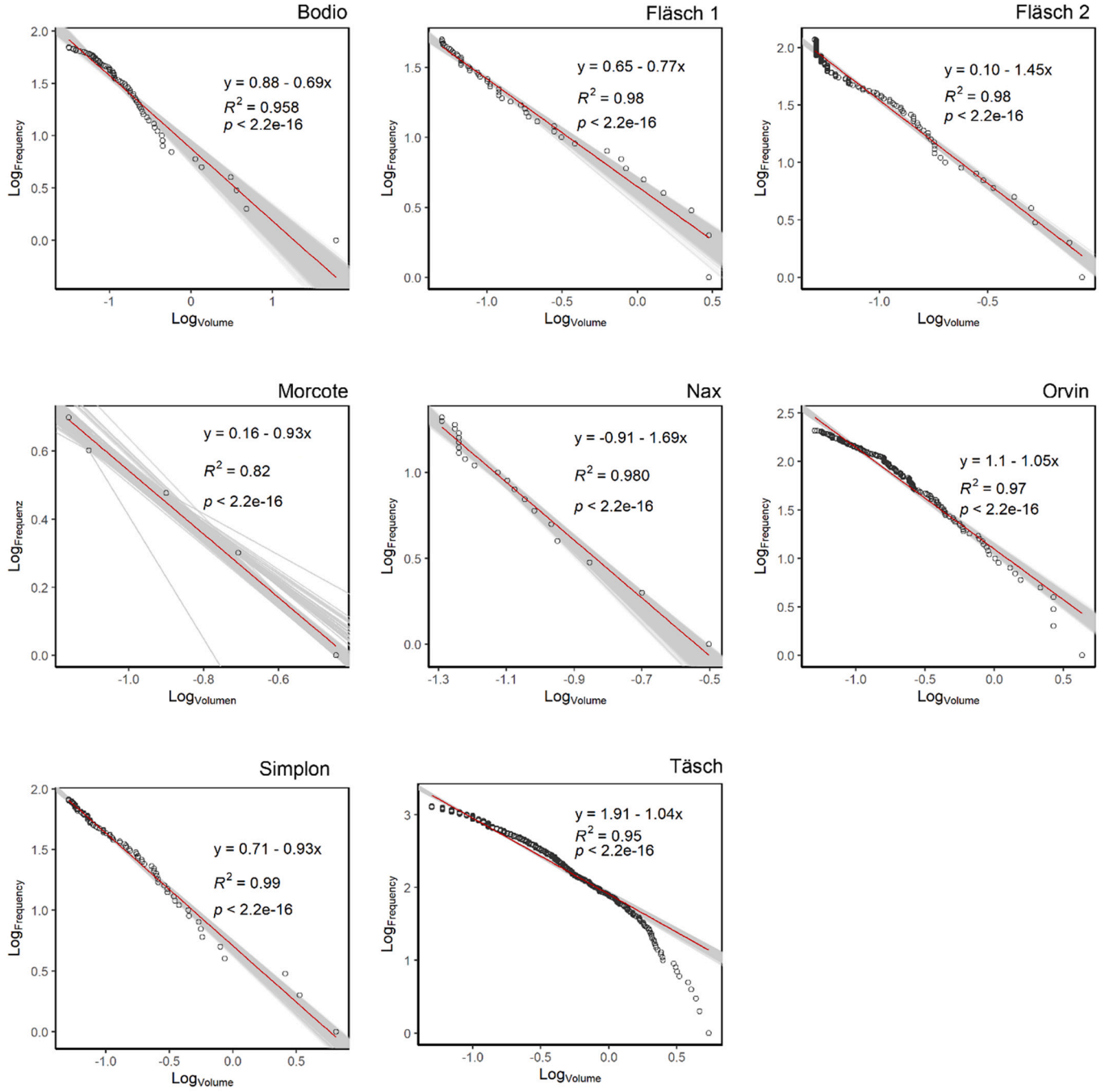

Fig. 6. Block volume distributions of the sampled blocks per site (with logarithmic axes), fitted linear regression (red) with coefficients and the bootstrapped regression models (grey). (For interpretation of the references to colour in this figure legend, the reader is referred to the web version of this article.)

and assuming that a sufficient number of deposited blocks is available. The comparison of fitted *b* values for different transects at two sites (Appendix B) exemplifies that the representativeness of the selected transects for the total block size distribution is more important than the number of measured blocks. It is thus difficult to indicate a minimum number of blocks to be measured. In case of large screes, measuring multiple transects representing different homogeneous deposition zones (cf. Ruiz-Carulla et al., 2015) is required. The comparison of the *b* and *B* values indicates a positive relationship between the two parameters, meaning that an increasing fracturing of the rock mass (increasing *B*) also results in a stronger fragmentation of the released volumes. Pursuing the systematic assessment of *b* values for other sites and for different geologies will possibly underpin potential relationships between the parameters and the main geological units.

The temporal frequencies and the volumes for different return periods depend on the release area and they increase with the considered cliff width. The comparison with the scenarios of the hazard assessments shows that the latter not always considered or underestimated the influence of the cliff size, since the difference between the RFM scenarios and the scenarios of the hazard assessments increase with increasing cliff size. The temporal frequencies and the volumes for different return periods depend on the height and the width of the considered cliff. Usually, the entire height of the cliff has to be considered, whereas the width to consider depends on the element at risk, which is not necessarily affected by the entire width of the cliff. For example, it may be the length of a road that run under the cliff. The occurrence frequency for

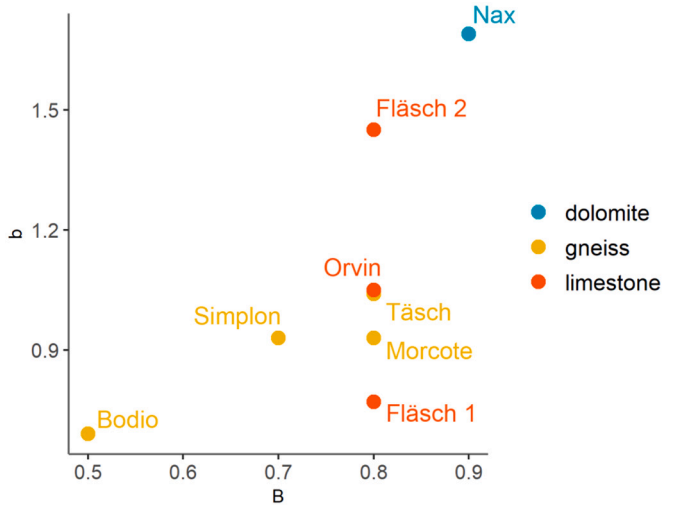

Fig. 7. Uniformity parameters for blocks (b) and rockfalls (B) of the 8 sites per main geological unit (dolomite, gneiss, limestone).

different block volumes at the element at risk finally depends on their spatio-temporal release frequencies and their probabilities of reaching the element at risk (e.g., Corominas et al., 2005; Hantz et al., 2016, 2017, 2021; Moos et al., 2018).

In case the RFM takes rare events into account or if the long-term erosion rate of a cliff shall be estimated, it is further necessary to estimate a maximum possible rockfall volume. We here used a rather simple approach since little data on the cliff structure was available. Mavrouli and Corominas (2020) proposed a probabilistic methodology to assess the penetration of sliding planes into the slope, which is expected to deliver more precise results.

The sensitivity and uncertainty analysis revealed a high variability of the release scenarios with respect to the parameters of the RFM, increasing with the return period. Both, the rockfall event volumes and the block volumes, are particularly sensitive to the parameter B. Only the sites of Morcote and Orvin had the largest uncertainty coefficients for the parameter A_{st} for return periods between 10 and 100 yrs. This can be explained by the relatively small cliff sizes of these sites and thus an increasing $V(F_t)$ with increasing B for small return periods (see Eq. 9 and Appendix C).

Variations in the range of one or half a class width in the structure classification scheme for the determination of parameter *B* can result in large variations of the rockfall or block volume, especially for rare events (return period >100 yrs.; Appendix C). A more unambiguous and simple applicable method to determine parameter *B* is required for a practical implementation of the RFM. Additionally, the *B* parameters have to be further tested for their validity, since the classification scheme was developed based on inventory data from different sites in France, mainly limestone cliffs (Hantz et al., 2020) and might not be equally valid for the considered sites.

The main drawback of the here proposed rockfall frequency model is the difficulty to validate it properly since long-term measurements of release frequencies are generally rare. The expert-based release scenarios used for comparison in this study are themselves subject to many uncertainties and thus cannot be regarded as "true value". A comparison to inventory data is also difficult since the rarely available data series are generally short and incomplete. Furthermore, information on block/event volumes is often unprecise (i.e., only estimated in classes or unclear whether block or event volume). Finally, rockfall inventories usually cover only events in the deposition area (or even only events that caused damages) and are thus rather representative for the occurrence frequency at the element at risk and not the release frequency. Nevertheless, the RFM is a promising and straightforward method to determine rockfall release scenarios where inventory data is scarce. Further testing at a wide variety of sites and for long-term observations (in the best case) could help increasing its robustness.

Table 4
Calculated rockfall release volumes ($V(F_t)$) for the four considered return periods (a = 10 yrs, b = 30 yrs, c = 100 yrs, d = 300 yrs), number of blocks with the maximum possible block volume and the maximum block volume for the respective rockfall release volumes, with medians and standard deviations calculated based on the Monte Carlo simulation. The last column shows the block volume scenarios estimated in the official hazard assessments (v_{hazard}) and determined based on other sources (for Orvin and Täsch).

Site	$V(F_t)$/ median/sd [m^3]	$n(v_{MAX})$/ median/sd	$v_{max}(F_t)$/ median/sd [m^3]	v_{hazard} [m^3] (other sources)
a)				
Bodio	**22**/29/182	0/0/0.2	**1**/2/43	0.4
Fläsch 1	**187**/226/512	1/1/3	**50**/42/15	10
Fläsch 2	**20**/25/28	0/0/0	**1**/2/1	1.125
Morcote	**0.5**/0.7/0.3	0/0/0	**0.1**/0.1/0.1	–
Nax	**15**/18/14	0/0/0	**0.8**/0.9/0.4	0.3
Orvin	**2**/3/1	0/0/0	**0.3**/0.3/0.2	0.5 (1.4)
Simplon	**21**/26/41	0/0.1/0.1	**3**/4/6	0.1
Täsch	**57**/71/108	0/0.2/0.3	**7**/8/11	7.5 (50)
b)				
Bodio	**199**/264/4694	0/0.3/7	**32**/48/43	3
Fläsch 1	**738**/882/2900	4/5/16	**50**/49/9	15
Fläsch 2	**81**/94/169	0/0.1/0.2	**4**/4/4	2.25
Morcote	**2**/3/2	0/0/0	**0.3**/0.3/0.2	–
Nax	**49**/59/65	0/0/0	**2**/2/1	0.3
Orvin	8/10/8	0/0/0	**1**/1/1	1.2 (7.4)
Simplon	**99**/125/339	0/0.4/1	**15**/19/18	0.5
Täsch	**226**/280/628	0/1/2	**25**/31/17	7.5 (50)
c)				
Bodio	**2210**/2883/13,787	2/3/33	**300**/264/101	20
Fläsch 1	**3326**/3921/9423	18/22/114	**50**/50/9	21
Fläsch 2	**360**/428/1138	0/0.5/1	**10**/12/12	5
Morcote	**13**/12/10	0/0.1/0.1	**2**/2/2	–
Nax	**187**/227/355	0/0/0	**4**/4/3	–
Orvin	**35**/41/55	0/0.3/0.4	**4**/5/6	3 (46)
Simplon	**552**/682/5993	2/2/12	**50**/46/13	5
Täsch	**1019**/1238/5599	2/3/10	**50**/47/11	15 (50)
d)				
Bodio	**19,881**/26,033/46,474	22/301/12,203	**300**/297/54	270
Fläsch 1	**13,133**/15,857/10,682	72/88/685	**50**/50/9	256 (event)
Fläsch 2	**14,223**/1716/6150	2/2/8	**20**/18/4	256 (event)
Morcote	**62**/45/60	0/1/1	**11**/8/7	–
Nax	**635**/755/1667	0/0.2/0.6	8/8/5	3
Orvin	**136**/164/322	0/1/2	**15**/18/16	9 (50)
Simplon	**2649**/3249/137′686	9/11/99	**50**/50/9	5
Täsch	**4023**/4882/143′000	9/11/59	**50**/50/9	–(50)

Funding

This research did not receive any specific grant from funding agencies in the public, commercial, or not-for-profit sectors.

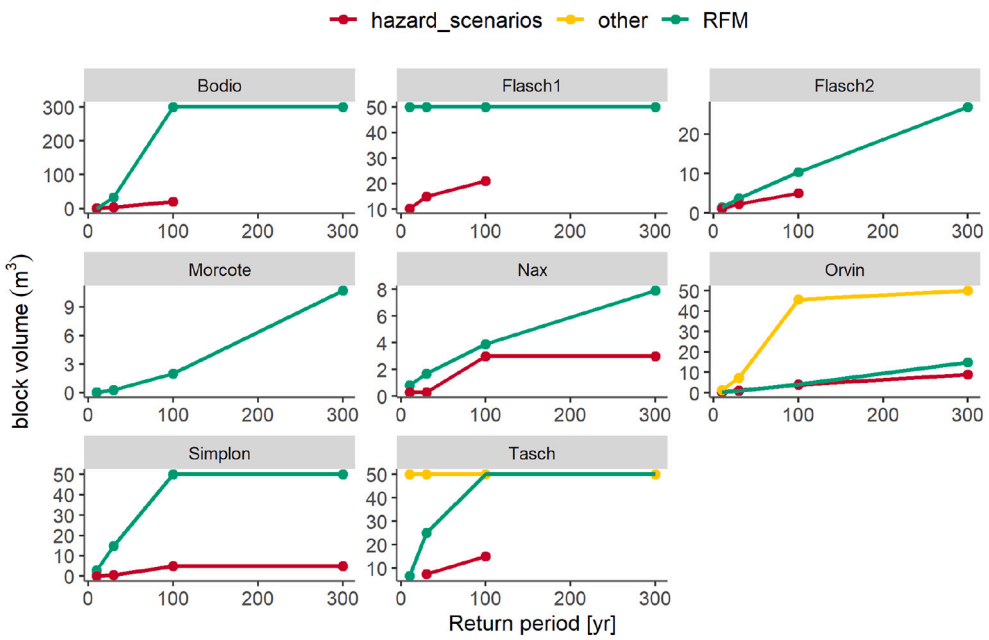

Fig. 8. Maximum block volumes per return period scenario and site calculated with the RFM (green) and block volume scenarios of the hazard assessments (red; where available) and calculated from other data for Täsch and Orvin (yellow). (For interpretation of the references to colour in this figure legend, the reader is referred to the web version of this article.)

Declaration of Competing Interest

The authors declare that they have no known competing financial interests or personal relationships that could have appeared to influence the work reported in this paper.

Appendix A. Rock cliffs of the 8 study sites

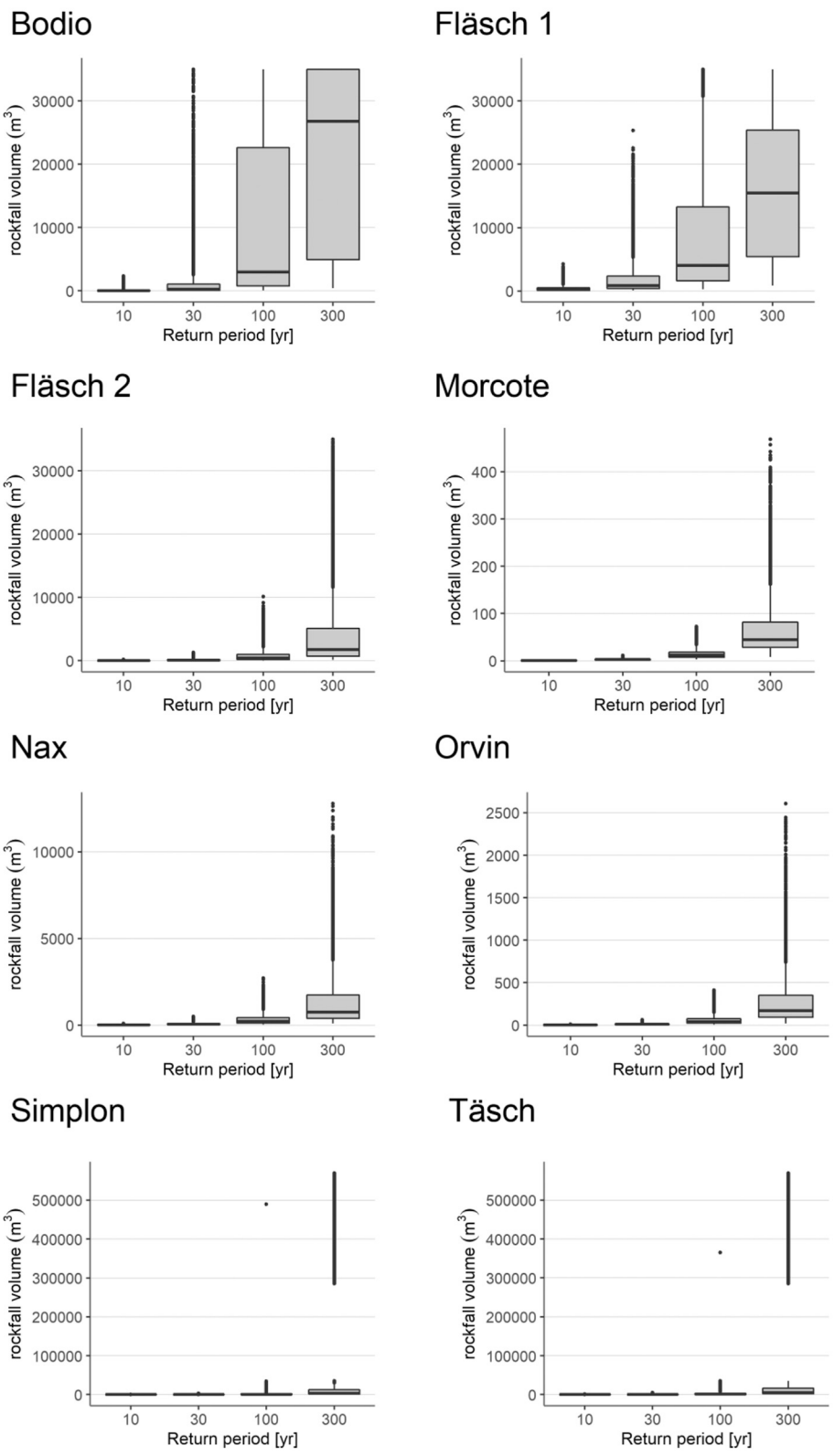

Fig. 9. Boxplots of the distribution of rockfall event volumes per release scenario (return period = 10, 30, 100, 300 yrs) and site calculated in the Monte Carlo simulation.

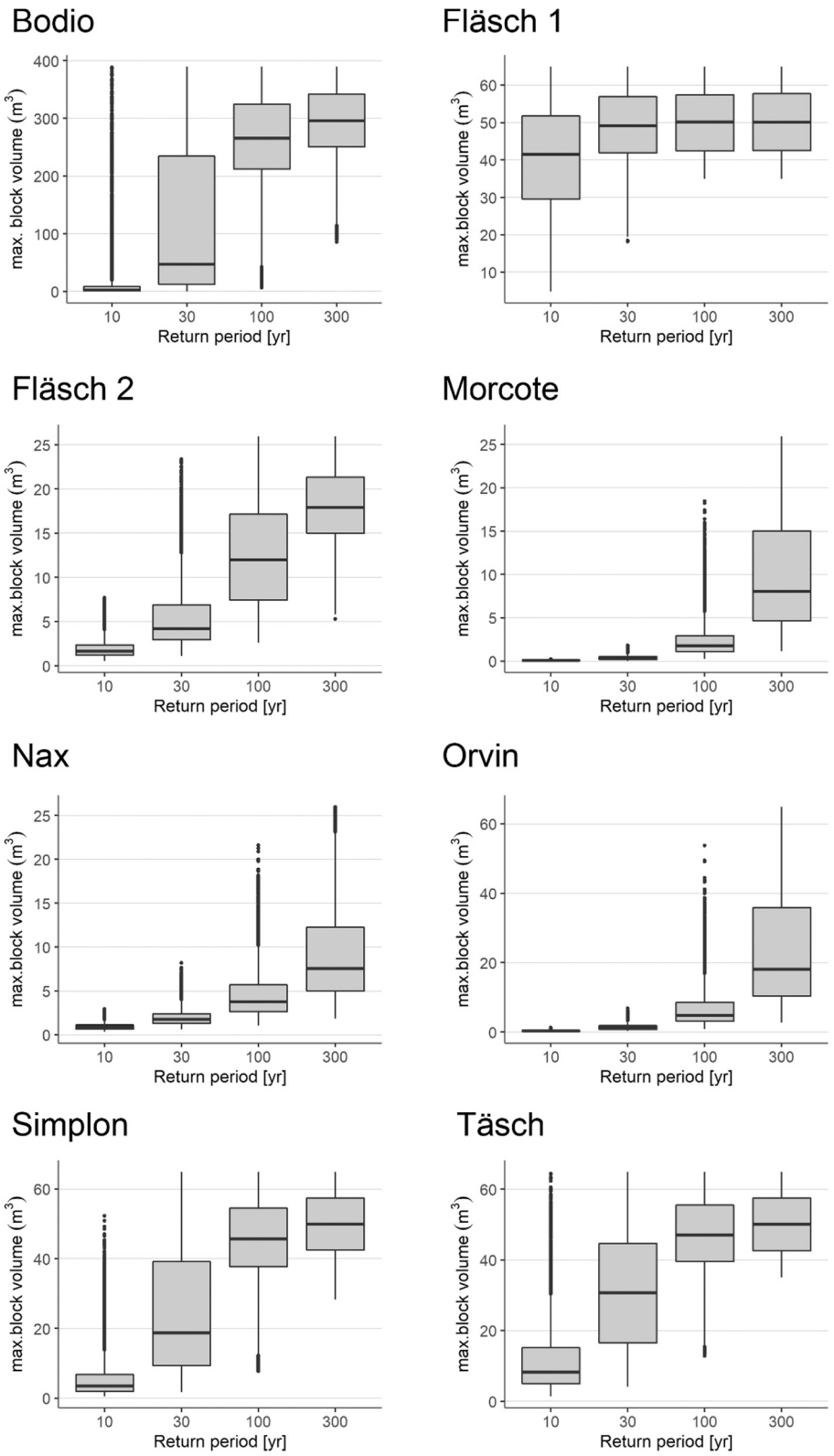

Fig. 10. Boxplots of the distribution of maximum block volumes of rockfall events of the release scenarios (return period = 10, 30, 100, 300 yrs) and site calculated in the Monte Carlo simulation.

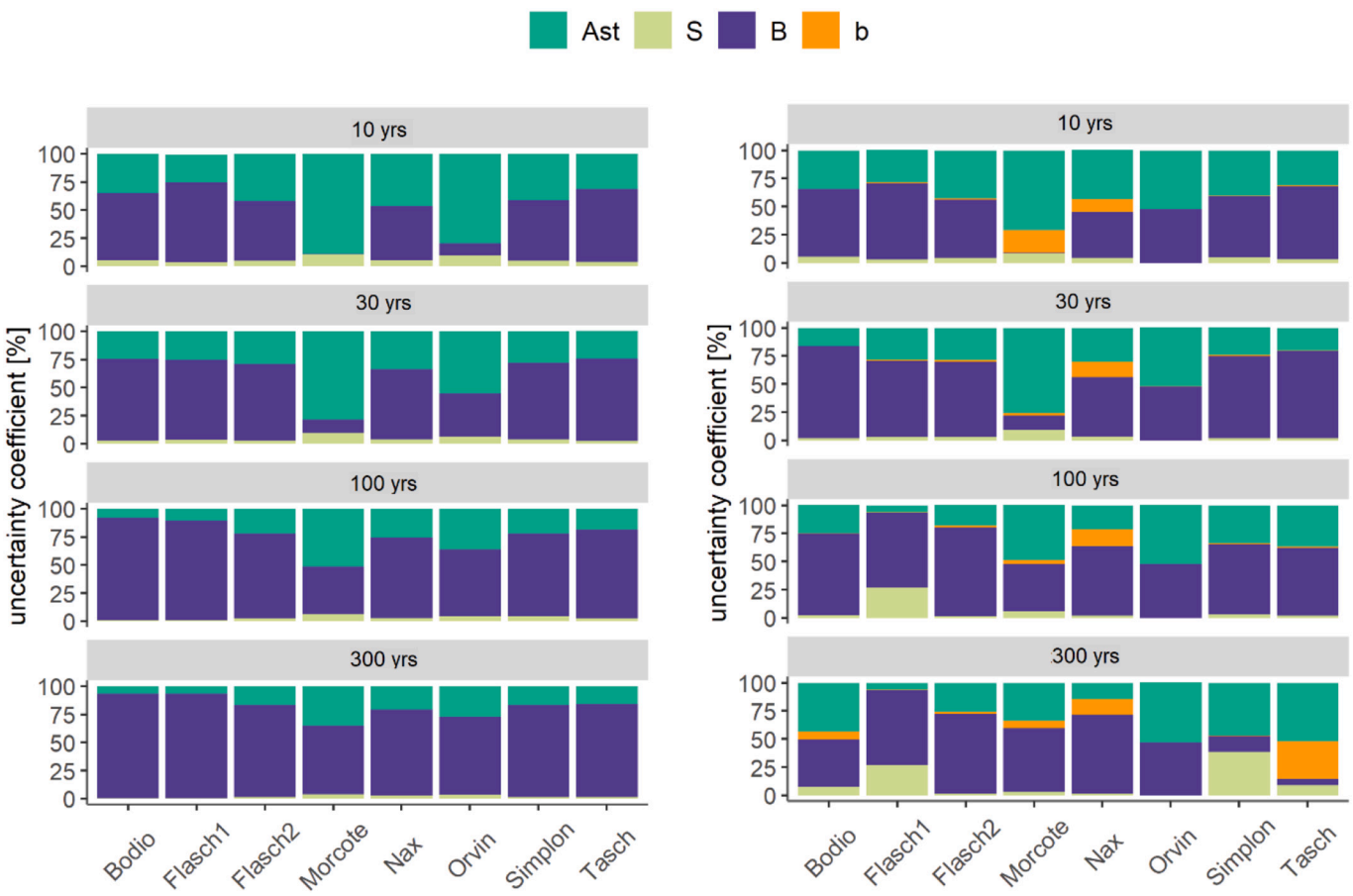

Fig. 11. Uncertainty coefficients (UC) of the variables of the Monte Carlo simulation for the rockfall event volumes (left) and maximum block volumes per event (right) per site and for the four return period scenarios. The UC were calculated based on least square linearization (Lei and Schilling, 1996) and show the uncertainty contribution of the respective variables on the output variance.

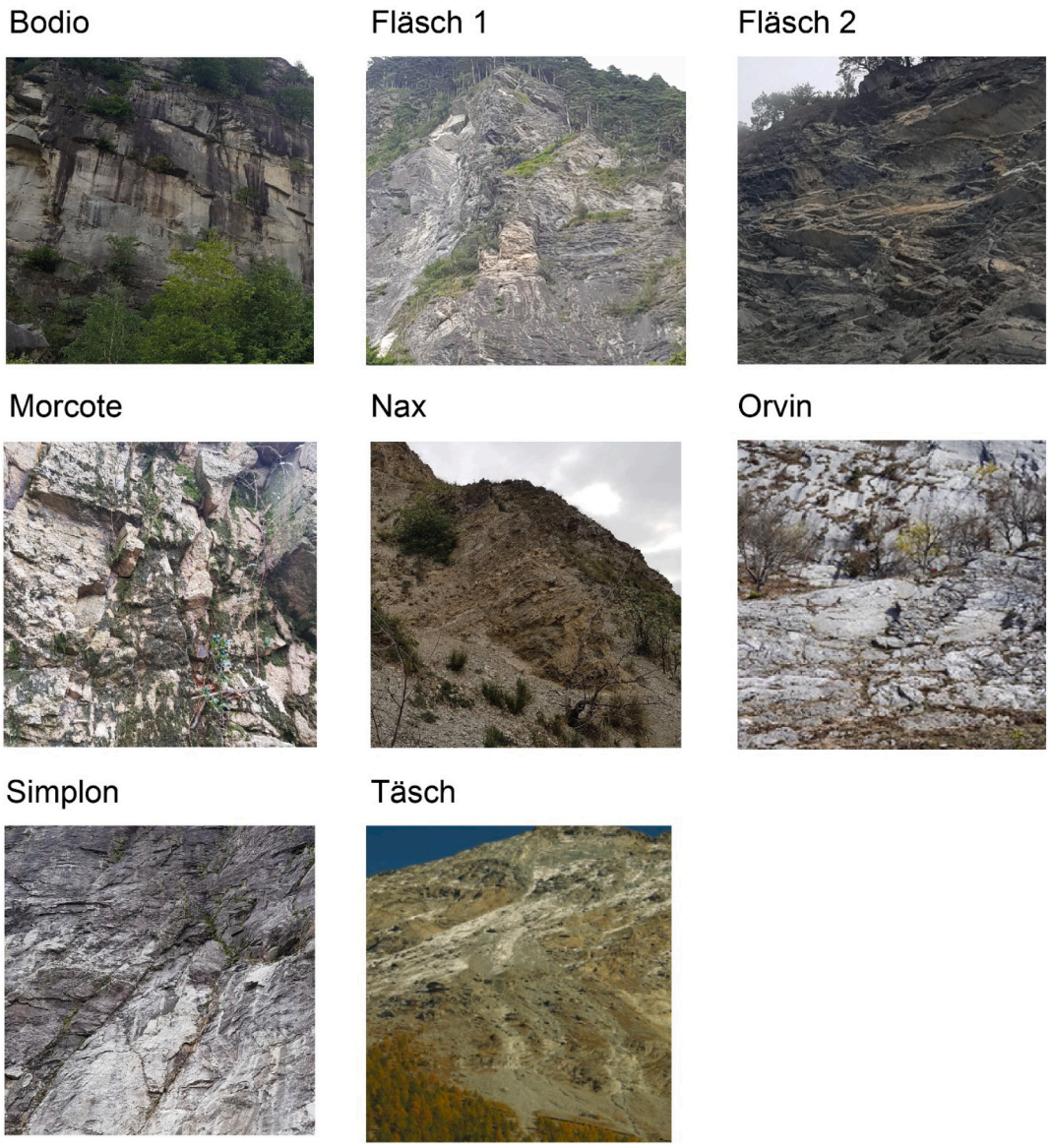

Fig. A.1: Photographs of the rock cliffs at the 8 study sites.

Appendix B. Comparison of fitted block size distributions based on multiple transects

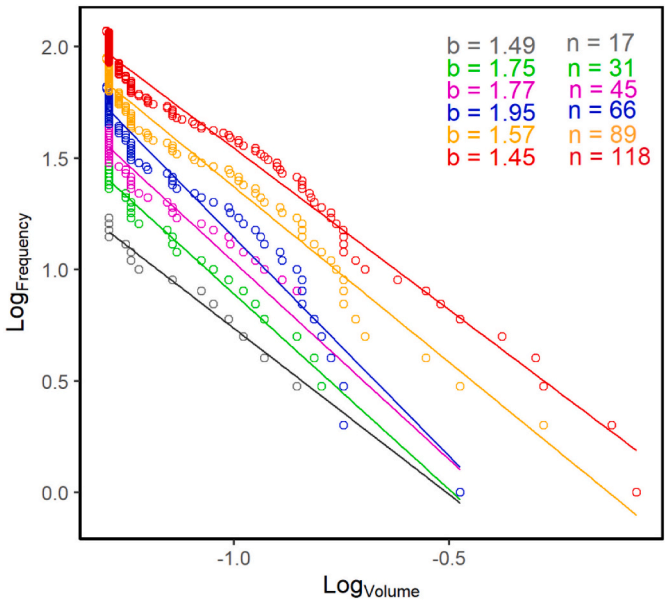

Fig. B.1: Block volume distributions and b values of an increasing number of transects for the site Fläsch 2. Red is the combination of all six transects. *n* gives the number of blocks per block volume distribution. (For interpretation of the references to colour in this figure legend, the reader is referred to the web version of this article.)

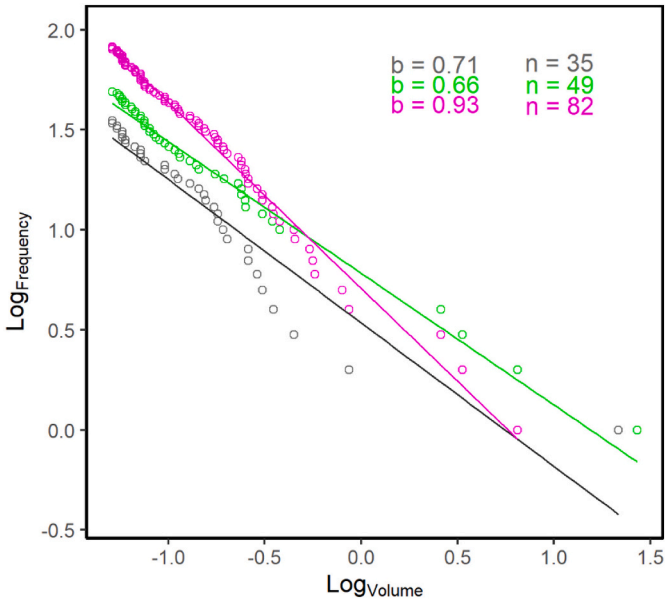

Fig. B.2: Block volume distributions and b values of two transects (grey, green) and all three transects combined (magenta) for the site Simplon. *n* gives the number of blocks per block volume distribution. (For interpretation of the references to colour in this figure legend, the reader is referred to the web version of this article.)

Appendix C. Rockfall event volume as function of the RFM parameters based on the Monte-Carlo simulation

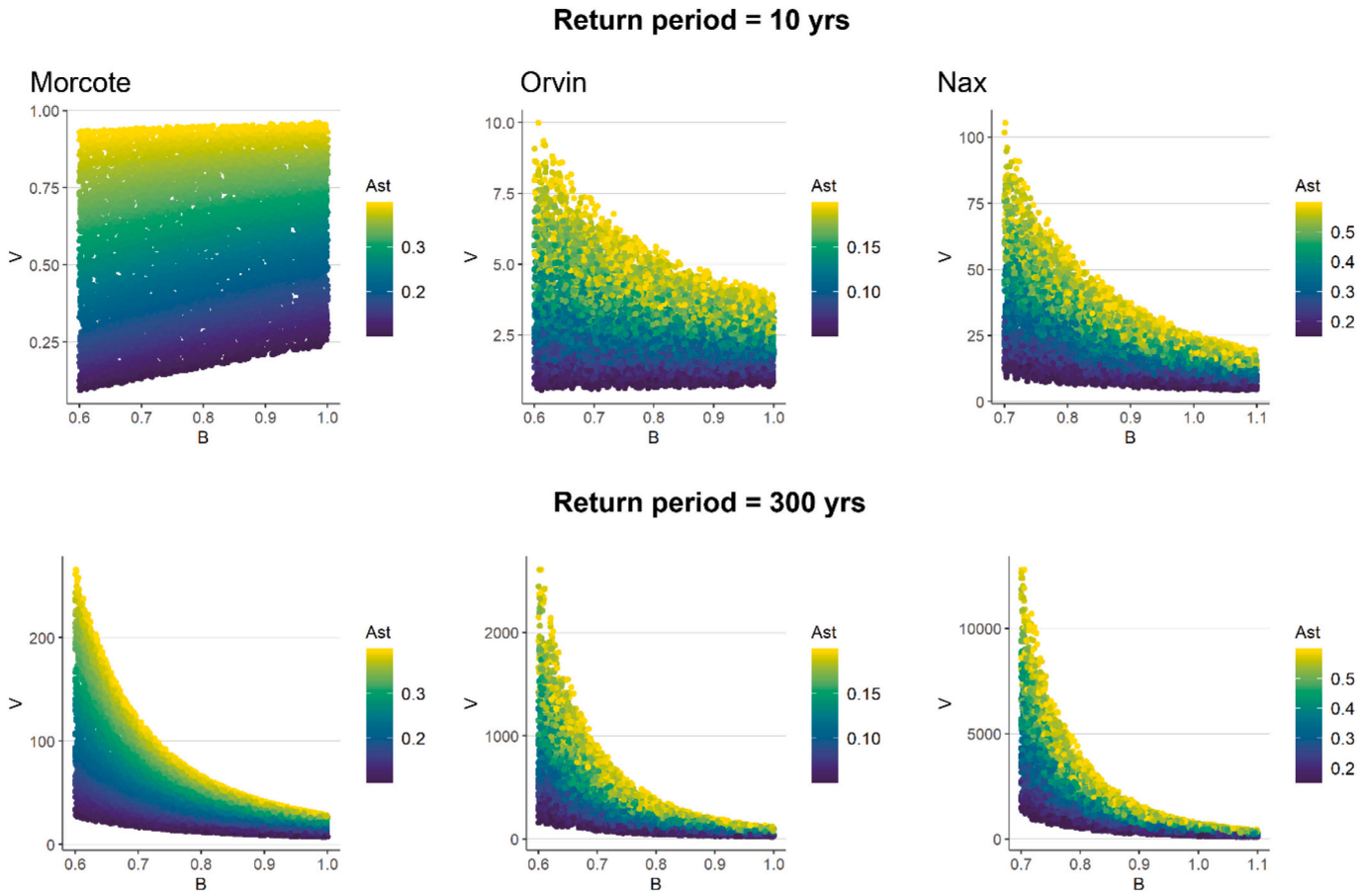

Fig. C.1: Rockfall event volume calculated in the Monte-Carlo simulation as function of parameter B (x-axis) and A_{st} (colour) for a return period of 10 (above) and 300 yrs. b(below) and the sites Morcote, Orvin and Nax.

References

Agliardi, F., Crosta, G.B., 2003. High resolution three-dimensional numerical modelling of rockfalls. Int. J. Rock Mech. Mining Sci. 40 (3), 455–471.

Allen, S.K., Cox, S.C., Owens, I.F., 2011. Rock avalanches and other landslides in the central Southern Alps of New Zealand: a regional study considering possible climate change impacts. Landslides 8 (1), 33–48.

Arnold, P., Dorren, Luuk, 2015. The importance of rockfall and landslide risks on Swiss national roads. In: Lollino, G., Giordan, D., Thuro, K., Carranza-Torres, C., Wu, F., Marinos, P., Delgado, C. (Eds.), Engineering Geology for Society and Territory. Springer International Publishing, Cham, pp. 671–675.

Bengoubou-Valérius, M., Gibert, D., 2013. Bootstrap determination of the reliability of b-values: an assessment of statistical estimators with synthetic magnitude series. In. Nat. Hazards 65 (1), 443–459. https://doi.org/10.1007/s11069-012-0376-1.

Bourrier, F., Dorren, L., Nicot, F., Berger, F., Darve, F., 2009. Toward objective rockfall trajectory simulation using a stochastic impact model. Geomorphology 110 (3–4), 68–79.

Brunetti, M.T., Guzzetti, F., Rossi, M., 2009. Probability distributions of landslide volumes. Nonlinear Process. Geophys. 16 (2), 179–188.

Christen, M., Bühler, Y., Bartelt, P., Leine, R., Glover, J., Schweizer, A., Graf, C., McArdell, B.W., Gerber, W., Deubelbeiss, Y., Feistl, T., Volkwein, A., 2012. Integral hazard management using a unified software environment. In: In Conference Proceedings of 12th Congress INTERPRAEVENT, pp. 77–86. Available online at. http://www.interpraevent.at/palm-cms/upload_files/publikationen/tagungsbeitraege/2012_1_77.pdf.

Corominas, J., Copons, R., Moya, J., Vilaplana, J.M., Altimir, J., Amigó, J., 2005. Quantitative assessment of the residual risk in a rockfall protected area. Landslides 2, 343–357.

Corominas, J., Mavrouli, O., Ruiz-Carulla, R., 2018. Magnitude and Frequency relations: are there geological constraints to the rockfall size? Landslides 15 (5), 829–845, 17p. https://doi.org/10.1007/s10346-017-0910-z.

De Biagi, V., Napoli, M.L., Barbero, M., Peila, D., 2017. Estimation of the return period of rockfall blocks according to their size. Nat. Hazards Earth Syst. Sci. 17, 103–113. https://doi.org/10.5194/nhess-17-103-2017.

De Blasio, F.V., Crosta, G.B., 2015. Fragmentation and boosting of rock falls and rock avalanches. Geophys. Res. Lett. 42 (20), 8463–8470.

Dorren, L., Berger, F., Putters, U.S., 2006. Real-size experiments and 3-D simulation of rockfall on forested and non-forested slopes. Natural Hazards Earth Syst. Sci. 6, 183–195. https://doi.org/10.1016/j.foreco.2005.05.012.

Dussauge-Peisser, C., Helstetter, A., Grasso, J.R., Hantz, D., Desvarreux, P., Jeannin, M., Giraud, A., 2002. Probabilistic approach to rock fall hazard assessment: potential of historical data analysis. In Nat. Hazards Earth Syst. Sci. 2, 15–26.

Eckert, N., Mainieri, R., Bourrier, F., Giacona, F., Corona, C., Le Bidan, V., Lescurier, A., 2020. Une base de données événementiele du risque rocheux dans les alpes françaises. Revue Franc. Geotech. 163 (3).

Farvacque, M., Corona, C., Lopez-Saez, J., Mainieri, R., Stoffel, M., Bourrier, F., Ecker, N., Toe, D., 2021. Estimating rockfall release frequency from blocks deposited in protection barriers, growth disturbances in trees, and trajectory simulations. Landslides. https://doi.org/10.1007/s10346-021-01719-0.

Ferrari, F., Giacomini, A., Thoeni, K., 2016. Qualtitative rockfall hazard assessment: a comprehensive review of current practices. Rock Mech. Rock. Eng. 49 (7), 2865–2922.

Frayssines, M., Hantz, D., 2006. Failure mechanisms and triggering factors in calcareous cliffs of the Subalpine Ranges (French Alps). Eng. Geol. 86, 256–270.

Guerin, A., Hantz, D., Rossetti, J.-P., Jaboyedoff, M., 2014. Brief Communication "Estimating Rockfall Frequency in a Mountain Limestone Cliff Using Terrestrial Laser Scanner".

Guzzetti, F., 2000. Landslide fatalities and the evaluation of landslide risk in Italy. Eng. Geol. 58, 89–107.

Hantz, D., Vengeon, J.M., Dussauge-Peisser, C., 2003a. An historical, geomechanical and probabilistic approach to rock-fall hazard assessment. Nat. Hazards Earth Syst. Sci. 3, 693–701.

Hantz, D., Dussauge-Peisser, C., Jeannin, M., Vengeon, J.-M., 2003b. Rock fall hazard assessment: from qualitative to quantitative failure probability. In: Int. conf. On Fast Slope Movements, Naples, 11-13 May 2003, pp. 263–267.

Hantz, D., Ventroux, Q., Rossetti, J.-P., Berger, F., 2016. A new approach of diffuse rockfall hazard. In: Aversa, et al. (Eds.), Landslides and Engineered Slopes. Associazione Geotecnica Italiana, Rome, Italy, pp. 1063–1067. ISBN 978-1-138-02988-0.

Hantz, D., Rossetti, J.-P., Valette, D., Bourrier, F., 2017. Quantitative rockfall hazard assessment at the Mont Saint-Eynard (French Alps). In: 6th Interdisciplinary Workshop on Rockfall Protection, May 22–24, 2017, Barcelona, Spain, p. 4.

Hantz, D., Colas, B., Dewez, T., Levy, C., Rosseti, J.-P., Guerin, A., Jaboyedoff, M., 2020. Quantitative assessment of rockfall release frequency. Rev. Fr. Géotech. 163, 2.
Hantz, D., Corominas, J., Crosta, G.B., Jaboyedoff, M., 2021. Definitions and concepts for quantitative rockfall hazard and risk analysis. Geosciences 2021 (11), 158. https://doi.org/10.3390/geosciences11040158.
Hoek, E., 2007. Rock mass properties. In: Practical Rock Engineering, chapter 11. Available from. http://www.rocscience.com/education/hoeks_corner (last consult: 2021/01/19).
Hoek, E., Bray, J.W., 1981. Rock slope engineering. In: London, the Institution of Mining and Metallurgy, London, UK.
Hoek, E., Marinos, P., 2000. Predicting tunnel squeezing. In: Tunnels and tunnelling international. Part 1 November Issue 2000. p. 45–51; Part 2—December 2000, pp. 34–36.
Hoek, E., Marinos, P.G., Marinos, V.P., 2005. Characterisation and engineering properties of tectonically undisturbed but lithologically varied sedimentary rock masses. Int. J. Rock Mech. Min. Sci. 42, 277–285.
Hungr, O., Evans, S., Hazzard, J., 1999. Magnitude and frequency of rock falls and rock slides along the main transportation corridors of southwestern British Columbia. Canad. Geotech. J. 36, 224–238.
Jaboyedoff, M., Couture, R., Locat, P., 2009. Structural analysis of Turtle Mountain (Alberta) using digital elevation model: towards a progressive failure. Geomorphology 103 (2009), 5–16. https://doi.org/10.1016/j.geomorph.2008.04.012.
Jaboyedoff, M., Carrea, D., Derron, M.-H., Oppikofer, T., Penna, I.M., Rudaz, B., 2020. A review of methods used to estimate initial landslide failure surface depths and volumes. Eng. Geol. 2020 (267), 105478.
Lanfranconi, C., Sala, G., Frattini, P., Crosta, G.B., Valagussa, A., 2020. Assessing the rockfall protection efficiency of forests at the regional scale. Landslide 17, 2703–2721. https://doi.org/10.1007/s10346-020-01458-8.
Lari, S., Frattini, P., Crosta, G.B., 2014. A probabilistic approach for landslide hazard analysis. Eng. Geol. 182 (Part A), 3–14. DOI: 10.16/j.enggeo.2014.07.015.
Lei, J.H., Schilling, W., 1996. Preliminary uncertainty analysis - a prerequisite for assessing the predictive uncertainty of hydrological models. Water Sci. Technol. 33, 79–90.
Lin, Q., Wang, Y., Xie, Y., Cheng, Q., Denk, K., 2022. Multiscale effects caused by the fracturing and fragmentation of rock blocks during rock mass movement: implications for rock avalanche propagation. Nat. Hazards Earth Syst. Sci. 22, 639–657.
Loew, S., Hantz, D., Gerber, W., 2021. Rockfall causes and transport mechanisms – A review. In: Earth Systems and Environmental Sciences. Reference Module in Earth Systems and Environmental SCIENCES, p. 32. https://doi.org/10.1016/B978-0-12-818234-5.00066-3.
Mainieri, R., Lopez-Saez, J., Corona, C., Stoffel, M., Bourrier, F., Eckert, N., 2019. Assessment of the recurrence intervals of rockfall through dendrogeomorphology and counting scar approach: a comparative study in a mixed forest stand form the Vercors massif (French Alps). Geomorphology 340, 160–171. https://doi.org/10.1016/j.geomorph.2019.05.005.
Marinos, P., Hoek, E., 2001. Estimating the geotechnical properties of heterogeneous rock masses such as flysch. Bull. Eng. Geol. Environ. 60, 85–92.
Mavrouli, O., Corominas, J., 2020. Evaluation of maximum rockfall dimensions based on probabilistic assessment of the penetration of the sliding planes into the slope. Rock Mech. Rock. Eng. 2020 (53), 2301–2312. https://doi.org/10.1007/s00603-020-02060-z.
Mavrouli, O., Corominas, J., Jaboyedoff, M., 2015. Size distribution for potentially unstable rock masses and in situ rock blocks using LIDAR-generated digital elevation models. Rock Mech. Rock. Eng. 48 (4), 1589–1604. https://doi.org/10.1007/s00603-014-0647-0.
Melzner, S., Rossi, M., Guzzetti, F., 2020. Impact of mapping strategies on rockfall frequency-size distributions. Eng. Geol. 272, 105639 https://doi.org/10.1016/j.enggeo.2020.105639.
Mohadjer, S., Ehlers, T.A., Nettesheim, M., Ott, M.B., Glotzbach, C., Drews, R., 2020. Temporal variations in rockfall and rock-wall retreat rates in a deglaciated valley over the past 11 k.y. Geology 48 (6), 594–598. https://doi.org/10.1130/G47092.1.
Moos, C., Fehlmann, M., Trappmann, D., Stoffel, M., Dorren, L., 2018. Integrating the mitigating effect of forests into quantitative rockfall risk analysis – two case studies in Switzerland. Intern. J. Disaster Risk Reduct. 32, 55–74. https://doi.org/10.1016/j.ijdrr.2017.09.036.
Ravanel, L., Deline, P., 2010. Climate influence on rockfalls in high-Alpine steep rockwalls: the north side of the Aiguilles de Chamonix (Mont Blanc massif) since the end of the "Little Ice Age". The Holocene 21, 357–365. https://doi.org/10.1144/1470-9236/05-008.
Ruiz Carulla, R., Matas, G., Prades, A., Gili, J.A., Corominas, J., Lantada, N., Buill, F., Mavrouli, O., Núñez, M.A., Moya, J., 2016. Analysis of rock block fragmentation by means of real-scale tests. In: Proceedings of the 3rd RSS, Rock Slope Stability conference, Lyon (France), pp. 107–108.
Ruiz-Carulla, R., Corominas, J., Mavrouli, O., 2015. A methodology to obtain the block size distribution of fragmental rockfall deposits. Landslides 12, 815–825. https://doi.org/10.1007/s10346-015-0600-7.
Ruiz-Carulla, R., Corominas, J., Mavrouli, O., 2017. A fractal fragmentation model for rockfalls. Landslides 14, 875–889.
Stoffel, M., Schneuwly, D., Bollschweiler, M., Lièvre, I., Delaloye, R., Myint, M., Monbaron, M., 2005. Analyzing rockfall activity (1600–2002) in a protection forest—a case study using dendrogeomorphology. Geomorphology 68 (3–4), 224–241. https://doi.org/10.1016/j.geomorph.2004.11.017.
Turcotte, D., 1986. Fractals and fragmentation. J. Geophys. Res. 91, 1921–1926.
Umili, G., Bonetto, S.M.R., Mosca, P., Vagnon, F., Ferrero, A.M., 2020. In Situ block size distribution aimed at the choice of the design block for rockfall barriers design: a case study along gardesana road. Geosciences 10 (6), 223. https://doi.org/10.3390/geosciences10060223.
van Veen, M., Hutchinson, D.J., Kromer, R., Lato, M., Edwards, T., 2017. Effects of sampling interval on the frequency - magnitude relationship of rockfalls detected from terrestrial laser scanning using semi-automated methods. Landslides. https://doi.org/10.1007/s10346-017-0801-3.
van Veen, M., Hutchinson, D.J., Bonneau, D.A., Sala, Z., Ondercin, M., Lato, M., 2018. Combining temporal 3-D remote sensing data with spatial rockfall simulations for improved understanding of hazardous slopes within rail corridors. In Nat. Hazards Earth Syst. Sci. 18 (8), 2295–2308. https://doi.org/10.5194/nhess-18-2295-2018.
Verbeeck, H., Samson, R., Verdonck, F., Lemeur, R., 2006. Parameter sensitivity and uncertainty of the forest carbon flux model FORUG: a Monte Carlo analysis. Tree Physiol. 26 (6), 807–817. https://doi.org/10.1093/treephys/26.6.807.
Williams, J.G., Rosser, N.J., Hardy, R.J., Brain, M.J., 2019. The Importance of monitoring Interval for Rockfall Magnitude-Frequency Estimation. Am. Geophys. Union. https://doi.org/10.1029/2019JF005225.